

Calculus detection for ultrasonography using decorrelation of forward scattered wave

Hirofumi Taki · Takuya Sakamoto ·
Makoto Yamakawa · Tsuyoshi Shiina ·
Toru Sato

Received: 30 September 2009 / Accepted: 25 March 2010 / Published online: 15 May 2010
© The Japan Society of Ultrasonics in Medicine 2010

Abstract

Purpose The purpose of this paper is to propose a novel strategy to detect small calculi efficiently.

Methods The proposed calculus detection strategy focuses on decorrelation of forward scattered waves caused by the failure of Born's approximation. A calculus causes waveform changes of transmit pulses, resulting in a decrease in the cross-correlation coefficients calculated from IQ signals scattered near the calculus position. Therefore, we can detect calculi from the appearance of dips in correlation coefficients.

Results When a calculus exists in a digital tissue map, sharp and deep dips in cross-correlation coefficients between acoustic IQ signals appear around the calculus. By contrast, no apparent dip exists when a tissue map contains no calculus. A scan line interval of 0.2 mm or less is appropriate for the conditions simulated in this paper, and the proper transmit focal range for the proposed method is at a calculus range.

Conclusion These results imply that the proposed strategy can improve the efficiency of US devices for small calculus detection.

Keywords Calculus detection · Forward scattered wave · Decorrelation · Ultrasonography · CFAR

Introduction

Ultrasonography (US) does not involve exposure to ionizing radiation and has an excellent ability to depict soft tissue, making it a convenient and effective clinical imaging tool. In contrast, US has poor sensitivity for detection of calculi compared with computed tomography (CT). Because the detection of calculi is important to distinguish between malignant masses and benign ones, the use of US is often an adjunct to other diagnostic tests [1–6].

A calculus is usually identified as a high-intensity echo with acoustic shadowing or enhancement [7, 8]. One strategy for detecting calculi is to detect high-intensity echoes in a B-mode image. This problem is equivalent to detecting targets in non-stationary noise and clutter while maintaining a constant probability of a false alarm. Finn et al. [9] designed a cell-averaging constant false alarm rate (CA CFAR) detector to set an adaptive threshold according to local noise levels. Hansen et al. [10] proposed a cell-averaging logarithmic constant false alarm rate (LOG CFAR) detector for operating over a larger dynamic range of background noise levels than the CA CFAR detector. To detect targets in an inhomogeneous medium, many researchers have reported several types of CFAR detectors [11, 12]. However, echo intensity from a small calculus is too low to detect it by simply selecting high-intensity echo masses.

Tissue harmonic imaging (THI) suppresses speckle artifacts utilizing harmonics, resulting in the improvement of contrast resolution [1, 13, 14]. THI thus helps to evaluate mass borders; however, it has insufficient calculus

H. Taki (✉) · T. Sakamoto · T. Sato
Graduate School of Informatics, Kyoto University,
Yoshida-honmachi, Sakyo-ku, Kyoto 606-8501, Japan
e-mail: hirofumi.taki@mb6.seikyou.ne.jp

M. Yamakawa
Advanced Biomedical Engineering Research Unit,
Kyoto University, Yoshida-honmachi, Sakyo-ku,
Kyoto 606-8501, Japan

T. Shiina
Graduate School of Medicine, Kyoto University,
Yoshida-honmachi, Sakyo-ku, Kyoto 606-8501, Japan

detectability compared with CT. By contrast, spatial compound imaging generates a single B-mode image from multiple sweeps [15, 16]. This technique improves image quality in terms of mass margins and internal architectures at the cost of a decrease in frame rate and suppression of acoustic shadowing [17]. Acoustic shadowing is one of the essential factors to detect small calculi, and thus compound imaging is inappropriate for calculus detection.

In general, US has difficulty depicting small calculi of 3.0 mm or less in size [2]. In addition, US depends heavily on operator skill. Conventional methods such as CFAR only provide information on backscattered waves from the ROI, and thus would theoretically hardly ever detect a small calculus when a high-echo target such as a layered structure exists close to the calculus. In this paper, we propose a calculus detection method employing the novel strategy to focus on decorrelation of forward scattered waves caused by the failure of Born's approximation. Since the proposed method detects a calculus using decorrelation of forward scattered waves, there is a good probability of detecting a small calculus from the waveform change in transmit waves caused by the calculus when the echo intensity of the calculus is too low to be detected by CFAR.

Materials and methods

Calculus detection using decorrelation of forward scattered waves

The proposed calculus detection strategy focuses on decorrelation of forward scattered waves caused by the failure of Born's approximation. For the investigation of decorrelation of forward scattered waves, we employed the cross-correlation between acoustic IQ signals of adjacent scan lines. Figure 1 shows the schema of this process. The cross-correlation coefficient behind a measurement point is

$$c(i,j) = \max_l g(i,j,l), \quad (1)$$

$$g(i,j,l) = \left| \sum_{J=j}^{j+L_w} e(i,J)e^*(i+1,J+l) \right| / \sqrt{p(i,j)p(i+1,j+l)}, \quad (2)$$

$$p(i,j) = \sum_{J=j}^{j+L_w} e(i,J)e^*(i,J), \quad (3)$$

where $e(i, j)$ is the IQ datum at E_{ij} , a pixel in a B-mode image, L_w is the correlation window width, and i and j are, respectively, the lateral and range coordinates in a B-mode image. When the medium is homogeneous and the layered structure is parallel to the skin surface, the maximization of $g(i, j, l)$ is not needed. We introduced the parameter l to

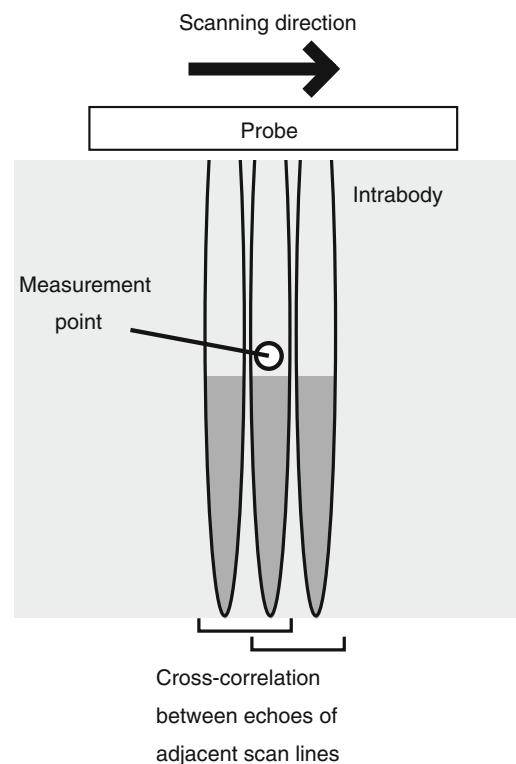


Fig. 1 Schema of the proposed calculus detection method using cross-correlation coefficients between two IQ signals of adjacent scan lines

suppress the path length difference between adjacent scan lines caused by the sound velocity variation in the medium and by the slope of a layered structure. In this study, two correlation windows were set with the depth ranges of 12.5–17.5 and 17.5–22.5 mm. When a small calculus exists in an acoustic beam, the waveform of a transmit wave changes because of several causes: creeping waves, a fast wave that goes through the calculus, diffraction, and multiple reflections in the calculus. Therefore, the echo waveform of a scan line with a calculus, returned from the inhomogeneous medium behind the calculus, was quite different from that without a calculus, as shown in Fig. 2. We can presume the existence of a calculus from the waveform difference between echoes of adjacent scan lines by calculating cross-correlation coefficients.

To equalize the influence of the noise among all cases with different simulation parameters, we calculated the average μ and standard deviation σ of cross-correlation coefficients by echoes scattered from positions more than 1 mm apart from the center, and then normalized the correlation coefficients using the averages and standard deviations.

Computer simulation with FDTD method

To evaluate the efficiency of the proposed calculus detection method, we employed PZFlex, a computer simulation

tool based on a finite-difference time-domain (FDTD) method [18, 19]. Here we set the grid size to 0.02 mm, satisfying the operating condition of PZFlex. In this simulation, a 19.1-mm-wide linear array probe was utilized. The probe had 32 elements, 0.5 mm wide, and an element gap of 0.1 mm. The center frequency of the transmit pulse was 4 MHz with a 60% fractional bandwidth.

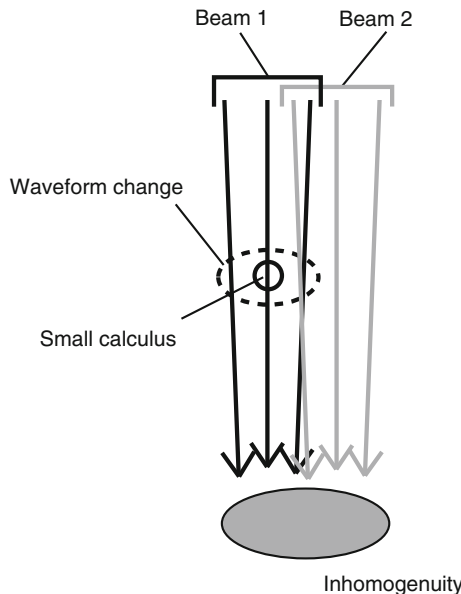
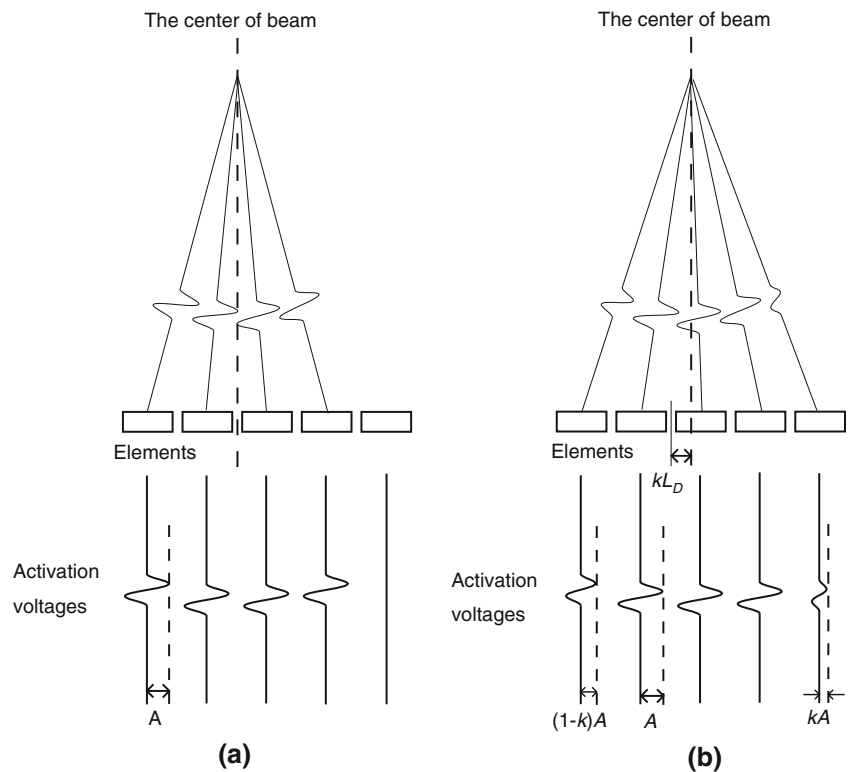


Fig. 2 Waveform change of a transmit pulse that originated from a calculus

Fig. 3 Schema of modification of input intensity for beamforming. **a** When a scan line is set at the center of an element gap, all activated elements radiate pulses with the same amplitude, where A denotes the amplitude. **b** When a distance exists between a scan line and the center of an element gap, the amplitudes of two pulses radiated from elements at both edges are modified to correspond to the distance, where L_D is the element interval and k is a real number satisfying $0 < k < 1$



Modification of input intensity for beamforming

To form a narrower scan line interval than the element interval, the input intensity of both edges of the activated elements are modified. As shown in Fig. 3, the amplitudes of transmit waves from both edge elements are controlled to correspond to the transmit beam position. When the center of the transmit beam is at the center of an element gap, 16 elements are activated, and all transmit pulses have the same amplitude. Otherwise, 17 elements are activated, and the amplitude of two transmit pulses radiated from both edge elements are modified, as shown in Fig. 3. At the transmit event, we employed four foci, fixed foci at 1, 1.5, and 2 cm depth, and dynamic focusing. By contrast, we utilized dynamic focusing at receive events with the same modification process.

Digital tissue map

To investigate the efficiency of the proposed calculus detection strategy, we prepared five simulated digital tissue maps with a calculus and five without a calculus. Figure 4 shows a digital tissue map with a calculus. The muscle layer, containing 5% minute fat droplets 0.1 mm in size, is located under skin that is 2 mm thick. A 0.5-mm-diameter calculus or a 1-mm-thick, 4-mm-wide connective tissue mass is embedded at the center at a depth of 10 mm, and a 1-mm-thick connective tissue layer is set at a depth of 15 mm.

Statistical analysis

We performed statistical analyses to compare two groups in terms of the dip depth of correlation coefficients using Student's *t* test.

Results

To survey the proper scan line interval and transmit the focal range for the proposed method, we examined the cross-correlation coefficients between the acoustic IQ signals of five digital tissue maps with a small calculus. Scan line intervals of 0.1, 0.2, 0.3, and 0.6 mm were used with

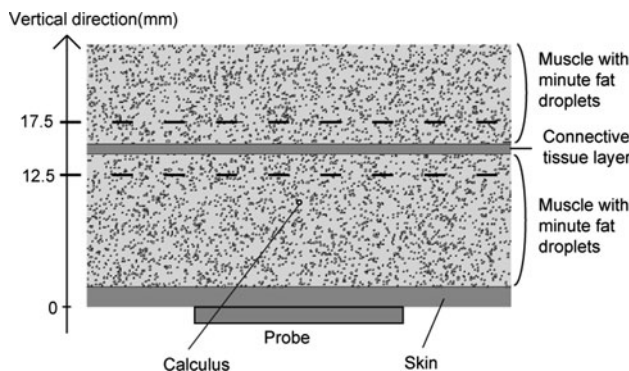
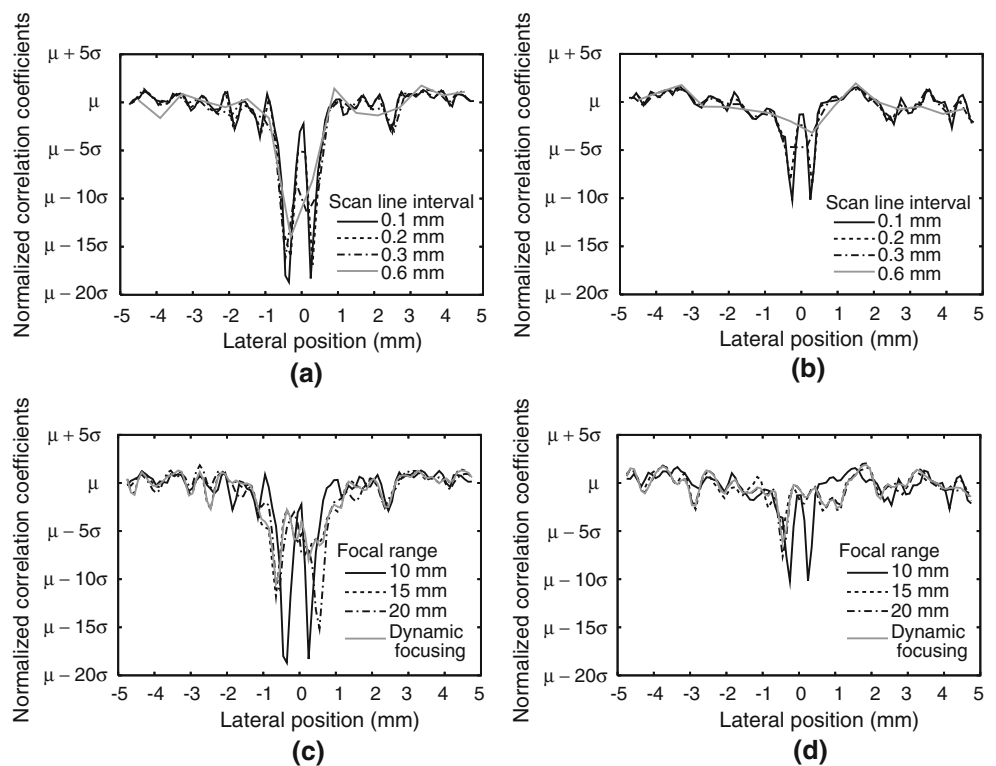


Fig. 4 Digital tissue map with a calculus

Fig. 5 Cross-correlation coefficients between two IQ signals of adjacent scan lines. **a** Comparison of correlation coefficients with respect to scan line intervals when the center of correlation windows are 15 mm and **b** 20 mm, where the transmit focal range is 10 mm. **c** Comparison of correlation coefficients with respect to transmit focal ranges when the center of correlation windows are 15 mm and **d** 20 mm, where the scan line interval is 0.1 mm

the transmit focus fixed at 10, 15, and 20 mm and dynamically changed. Figure 5 shows the cross-correlation coefficients obtained using a digital tissue map with a calculus. In all cases, dips of correlation coefficients appear around the center, i.e., the position of the calculus. These results indicate that the waveform changes of transmit pulses, which originate from a calculus, suppress correlation coefficients around the center. When the center of a correlation window was 15 mm deep, i.e., a correlation window with a layered structure, deeper dips appeared as compared with those when the center was 20 mm, where the level of significance for Student's *t* test is 0.005. Since the influence of noise among all cases with different simulation parameters was equalized by the normalization process using averages and standard deviation, we investigated proper parameters for the proposed calculus detection method using the minimum number of normalized correlation coefficients where their lateral positions are within 1 mm of the center.

Figure 6 shows the averages and standard deviations of dip depth of correlation coefficients around the center among five digital maps. When the transmit focal range was fixed at a depth of 10 mm, there was no statistical significance concerning the dips of correlation coefficients between scan line intervals of 0.1 and 0.2 mm, as shown in Fig. 6a. By contrast, when the center of the correlation window was 15 mm, dips of 0.3- and 0.6-mm scan line intervals were shallower than that of 0.1-mm scan line intervals, where the levels of significance for Student's *t*



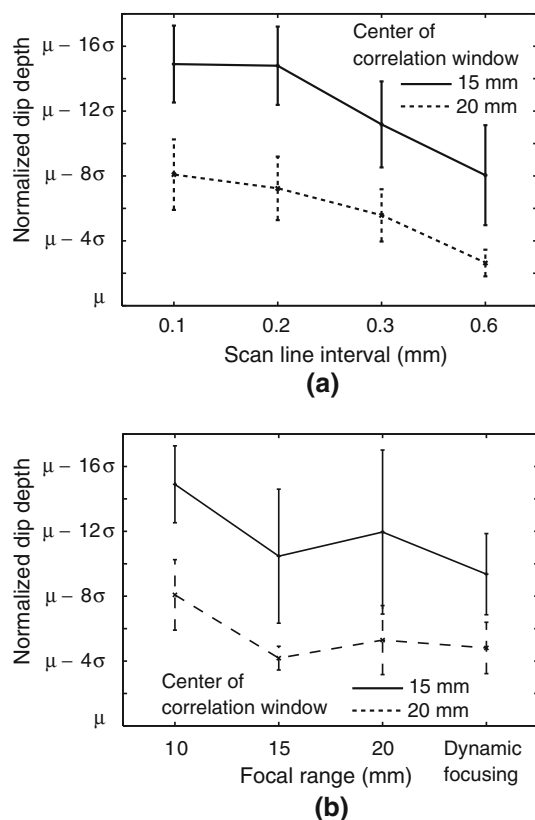


Fig. 6 Averages and standard deviations of dip depth of correlation coefficients around the calculus position. **a** Comparison of dip depth with respect to scan line intervals, where the transmit focal range is 10 mm. **b** Comparison of dip depth with respect to transmit focal ranges, where the scan line interval is 0.1 mm

tests are 0.05 and 0.005, respectively. As shown in Fig. 6b, when the scan line interval was 0.1 mm, a transmit beam with a fixed focal range of 10 mm, the calculus depth, resulted in the deepest dips of correlation coefficients with and without an echo from a layered structure in the signal cut out by a correlation window. In particular, the dynamic focusing for transmit beams deteriorated the conspicuousness of correlation dips. These results show that the proper scan line interval is 0.2 mm or less, and the focal range should be at the calculus depth.

A specular echo from a flat structure often interferes with the detection of a calculus in an US test. To confirm the ability of the proposed method to distinguish a calculus from a flat structure, we compared correlation coefficients of a digital tissue map with a calculus and that with a flat connective tissue mass. Figure 7 shows that dips of correlation coefficients appear only when a digital tissue map with a calculus is used, where the scan line interval is 0.1 mm and the focal range is set at 10 mm, the calculus depth. These results indicate the capability of the proposed method to detect a calculus in an inhomogeneous human body with several specular echoes.

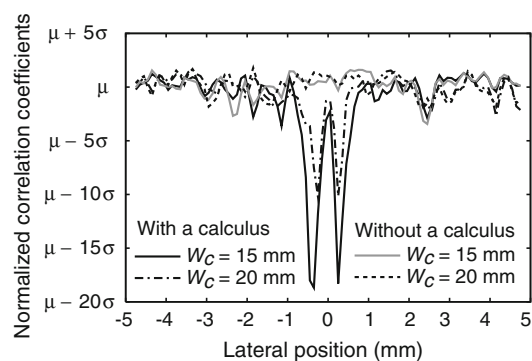


Fig. 7 Correlation coefficients of digital maps with and without a calculus. Dips of correlation coefficients appear only when there is a calculus, where W_c denotes the center of correlation windows

Discussion

In this study, we proposed a calculus detection method focusing on decorrelation of forward scattered waves caused by the failure of Born's approximation. We investigated the ability of the method by using a computer simulation, and optimized the scan line interval and the focal range of transmit beams. This study verified that a calculus creates dips in cross-correlation coefficients around the center; by contrast, a flat connective tissue mass does not. This result indicates that the proposed method has the capability to detect a small calculus 0.5 mm wide in an inhomogeneous human body.

A wide scan line interval decreases the overlap between two beams of adjacent scan lines, suppressing the correlation coefficients between IQ signals of adjacent scan lines. This conceals the decrease in correlation coefficients originating from a calculus. By contrast, when a scan line interval is sufficiently narrow to raise correlation coefficients of adjacent scan lines without a calculus to 1, a calculus creates dips in correlation coefficients, and the proposed method can then detect the calculus effectively. Therefore, for the proposed method a scan line interval should have an upper limit. Under the conditions simulated in this paper, the limit was about 0.2 mm.

When a scan line interval was sufficiently narrow, a calculus influenced multiple transmit beams, resulting in high cross-correlation coefficients located close to the calculus, as shown in Fig. 8. By contrast, when a transmit beam encountered a calculus, a correlation coefficient was calculated from two IQ signals with and without the waveform change caused by the calculus, creating a dip in correlation coefficients. Therefore, two dips in correlation coefficients appeared in cases where the scan line intervals were 0.1 and 0.2 mm. As shown in Fig. 9, a narrow beam at a calculus depth increases the waveform change of the beam caused by a calculus, resulting in deep dips in

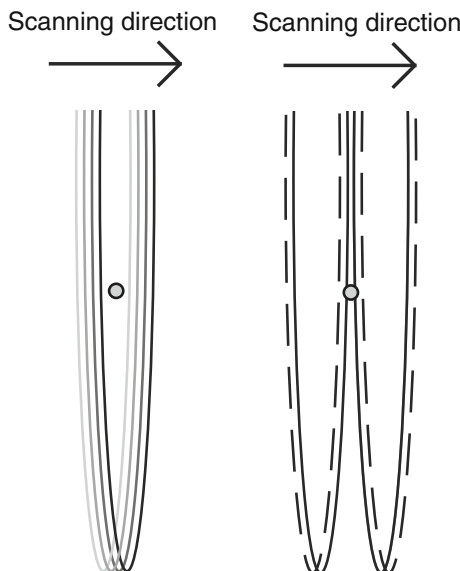


Fig. 8 Appearance of two dips of correlation coefficients calculated using a digital tissue map with a calculus. **a** When scan lines are located close to a calculus, waveform changes originating from the calculus occur in all the pulses of the scan lines. Therefore, the echoes of adjacent scan lines are similar in waveform, resulting in high correlation coefficients at the position close to the calculus. **b** When a transmit beam comes into contacts with a calculus, two IQ signals with and without a calculus in the beams adjoin, creating a dip in correlation coefficients

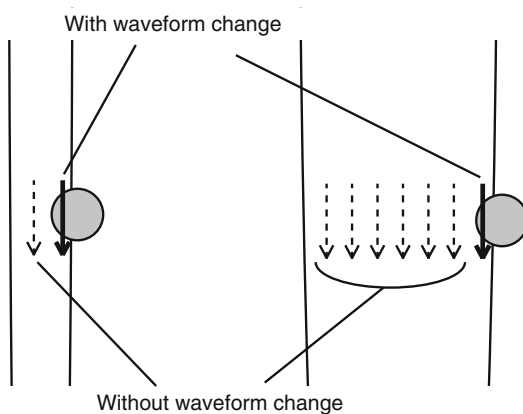


Fig. 9 Schema of waveform change that originated from a calculus comparing a narrow and wide transmit beam

correlation coefficients. Thus, the proper focal range for the proposed method is at calculus depth.

This paper described only the results of a simulation study and did not include any *in vitro* or *in vivo* data. There are several major hurdles that have to be overcome before clinical application of this technology.

In conclusion, we proposed a novel calculus detection method focusing on decorrelation of forward scattered

waves caused by the failure of Born's approximation, verified the efficacy of the method via computer simulation, and investigated a proper transmit focal range and scan line interval. The results imply the capability of the method to detect small calculi 0.5 mm in diameter in an inhomogeneous human body.

Acknowledgments This work was partly supported by the Research and Development Committee Program of the Japan Society of Ultrasonics in Medicine and the Innovative Techno-Hub for Integrated Medical Bio-imaging Project of the Special Coordination Funds for Promoting Science and Technology from the Ministry of Education, Culture, Sports, Science and Technology (MEXT), Japan.

References

- Özdemir H, Demir MK, Temizöz O, et al. Phase inversion harmonic imaging improves assessment of renal calculi: a comparison with fundamental gray-scale sonography. *J Clin Ultrasound*. 2008;36:16–9.
- Fowler KAB, Locken JA, Duchesne JH, et al. US for detecting renal calculi with nonenhanced CT as a reference standard. *Radiology*. 2002;222:109–13.
- Lamb PM, Perry NM, Vinnicombe SJ, et al. Correlation between ultrasound characteristics, mammographic findings and histological grade in patients with invasive ductal carcinoma of the breast. *Clin Radiol*. 2000;55:40–4.
- Jacob D, Brombart JC, Muller C, et al. Analysis of the results of 137 subclinical breast lesions excisions. Value of ultrasonography in the early diagnosis of breast cancer. *J Gynecol Obstet Biol Reprod (Paris)*. 1997;26:27–31.
- Mahnken AH, Mühlensbruch G, Das M, et al. MDCT detection of mitral valve calcification: prevalence and clinical relevance compared with echocardiography. *Am J Roentgenol*. 2007;188:1264–9.
- Liu F, Coursey CA, Grahame-Clarke C, et al. Aortic valve calcification as an incidental finding at CT of the elderly: severity and location as predictors of aortic stenosis. *Am J Roentgenol*. 2006;186:342–9.
- Janetschek G, Putz A, Feichtinger H. Renal transitional cell carcinoma mimicking stone echoes. *J Ultrasound Med*. 1988;7:83–6.
- Roesel GC, Toepfer NJ, Battino BS, et al. A calcified papillary renal cell carcinoma masquerading as a renal pelvic calculus. *Curr Urol*. 2007;1:217–8.
- Finn HM, Johnson RS. Adaptive detection mode with threshold control as a function of spatially sampled clutter-level estimates. *RCA Rev*. 1968;29:414–65.
- Hansen VG, Ward HR. Detection performance of the cell averaging LOG/CFAR receiver. *IEEE Trans Aerosp Electron Syst*. 1972;5:648–52.
- Zhu Y, Weight JP. Ultrasonic nondestructive evaluation of highly scattering materials using adaptive filtering and detection. *IEEE Trans Ultrason Ferroelect Freq Control*. 1994;41:26–33.
- Kamiyama N, Okamura Y, Kakee A, et al. Investigation of ultrasound image processing to improve perceptibility of microcalcifications. *J Med Ultrasonics*. 2008;35:97–105.
- Schmidt T, Hohl C, Haage P, et al. Diagnostic accuracy of phase-inversion tissue harmonic imaging versus fundamental B-mode sonography in the evaluation of focal lesions of the kidney. *Am J Roentgenol*. 2003;180:1639–47.
- Rosen EL, Soo MS. Tissue harmonic imaging sonography of breast lesions improved margin analysis, conspicuity, and image

- quality compared to conventional ultrasound. *Clin Imaging*. 2001;25:379–84.
15. Krücker JF, Meyer CR, LeCarpentier GL, et al. 3D spatial compounding of ultrasound imaging using image-based nonrigid registration. *Ultrasound Med Biol*. 2000;26:1475–88.
 16. Moskalik A, Carson PL, Meyer CR, et al. Registration of 3-dimensional compound ultrasound scans of the breast for refraction and motion correction. *Ultrasound Med Biol*. 1995;21:769–78.
 17. Weinstein SP, Conant EF, Sehgal C. Technical advances in breast ultrasound imaging. *Semin Ultrasound CT MR*. 2006;27:273–83.
 18. Hossack JA, Hayward G. Finite-element analysis of 1–3 composite transducers. *IEEE Trans Ultrason Ferroelect Freq Control*. 1991;38:618–29.
 19. Lerch R. Simulation of piezoelectric devices by two- and three-dimensional finite elements. *IEEE Trans Ultrason Ferroelect Freq Control*. 1990;37:233–47.